Human Epidermal Growth Factor Receptor 3–Specific Tumor Uptake and Biodistribution of ^{89}Zr-MSB0010853 Visualized by Real-Time and Noninvasive PET Imaging

Frank J. Warnders[1], Anton G.T. Terwisscha van Scheltinga[1], Christine Knuehl[2], Maarten van Roy[3], Erik F.J. de Vries[4], Jos G.W. Kosterink[5,6], Elisabeth G.E. de Vries[7], and Marjolijn N. Lub-de Hooge[1,4]

[1]Department of Clinical Pharmacy and Pharmacology, University of Groningen, University Medical Center Groningen, Groningen, The Netherlands; [2]Merck, Biopharma Global R&D, Darmstadt, Germany; [3]Ablynx N.V., Ghent, Belgium; [4]Department of Nuclear Medicine and Molecular Imaging, University of Groningen, University Medical Center Groningen, Groningen, The Netherlands; [5]Department of Clinical Pharmacy and Pharmacology, University Medical Center Groningen, Groningen, The Netherlands; [6]Unit PharmacoTherapy, Epidemiology and Economy, Groningen Research Institute of Pharmacy, University of Groningen, Groningen, The Netherlands; and [7]Department of Medical Oncology, University of Groningen, University Medical Center Groningen, Groningen, The Netherlands

The human epidermal growth factor receptor 3 (HER3) is an interesting target for antitumor therapy. For optimal HER3 signaling inhibition, a biparatopic Nanobody construct (MSB0010853) was developed that binds 2 different HER3 epitopes. In addition, MSB0010853 contains a third HER3 epitope that binds albumin to extend its circulation time. MSB0010853 is cross-reactive with HER3 and albumin of mouse origin. We aimed to gain insight into MSB0010853 biodistribution and tumor uptake by radiolabeling the Nanobody construct with ^{89}Zr. **Methods:** MSB0010853 was radiolabeled with ^{89}Zr. Dose- and time-dependent tumor uptake was studied in nude BALB/c mice bearing a subcutaneous HER3 overexpressing H441 non–small cell lung cancer xenograft. Dose-dependent biodistribution of ^{89}Zr-MSB0010853 was assessed ex vivo at 24 h after intravenous injection. Protein doses of 5, 10, 25, 100, and 1,000 μg were used. Time-dependent biodistribution of MSB0010853 was analyzed ex vivo at 3, 6, 24, and 96 h after intravenous administration of 25 μg of ^{89}Zr-MSB0010853. PET imaging and biodistribution were performed 24 h after administration of 25 μg of ^{89}Zr-MSB0010853 to mice bearing human H441, FaDu (high HER3 expression), or Calu-1 (no HER3 expression) tumor xenografts. **Results:** Radiolabeling of MSB0010853 with ^{89}Zr was performed with a radiochemical purity of greater than 95%. Ex vivo biodistribution showed protein dose– and time-dependent distribution of ^{89}Zr-MSB0010853 in all organs. Uptake of ^{89}Zr-MSB0010853 in H441 tumors was only time-dependent. Tumor could be visualized up to at least 96 h after injection. The highest mean SUV of 0.6 ± 0.2 was observed at 24 h after injection of 25 μg of ^{89}Zr-MSB0010853. ^{89}Zr-MSB0010853 tumor uptake correlated with HER3 expression and was highest in H441 (6.2 ± 1.1 percentage injected dose per gram [%ID/g]) and lowest in Calu-1 (2.3 ± 0.3 %ID/g) xenografts. **Conclusion:** ^{89}Zr-MSB0010853 organ distribution and tumor uptake in mice are time-dependent, and tumor uptake correlates with HER3 expression. In contrast to tumor uptake except for kidney uptake, organ distribution of ^{89}Zr-MSB0010853 is protein dose–dependent for the tested doses. ^{89}Zr-MSB0010853 PET imaging gives insight into the in vivo behavior of MSB0010853.

Key Words: imaging; ^{89}Zr; Nanobody; HER3; albumin

J Nucl Med 2017; 58:1210–1215
DOI: 10.2967/jnumed.116.181586

Members of the human epidermal growth factor receptor (HER) family, consisting of epidermal growth factor receptor (EGFR), HER2, HER3, and HER4, play a key role in tumor growth, differentiation, survival, metastasis, and angiogenesis (*1*). Incorrect signaling of EGFR and HER2 underlies the pathogenesis of a variety of cancers. Therefore, these prooncogenic receptors are targets of several therapies used for cancer treatment. Unfortunately, many patients do not respond to these drugs or experience tumor progression after an initial response.

Unlike other members of the family, HER3 has reduced kinase activity but can form highly activated heterodimers with EGFR and HER2. HER3 overexpression is associated with resistance against EGFR- and HER2-targeted therapy (*2*). In preclinical models, a combination of HER3-targeting antibodies with cetuximab, erlotinib, pertuzumab, trastuzumab, or lapatinib plus trastuzumab resulted in increased antitumor activity (*3–8*). Several clinical trials evaluate this approach as well (*9*).

Interestingly, a mixture of 2 anti-HER3 antibodies (A5 and F4) blocked ligand-induced and independent HER3 signaling and inhibited tumor cell growth better than each antibody alone (*10*). Blocking 2 different HER3 epitopes, with a biparatopic Nanobody construct (MSB0010853; Ablynx), is therefore an interesting option.

With their small size (15 kDa), high stability, and straightforward production, monovalent Nanobodies are ideal building blocks to develop biparatopic constructs (*11*). Nanobodies show rapid tumor penetration and fast renal clearance (*12*). MSB0010853 (39.5 kDa) consists of 2 HER3-targeting Nanobodies and an additional third that is able to bind albumin, extending its half-life (Figs. 1A and 1B). MSB0010853 binds HER3 at domain 1 and at a second unknown domain. All 3 Nanobodies target human and mouse antigen.

Currently, little information on the pharmacologic behavior of MSB0010853 is available. Molecular imaging can provide additional insight in biodistribution and tumor accumulation. Molecular

Received Oct. 5, 2016; revision accepted Mar. 8, 2017.
For correspondence or reprints contact: Marjolijn N. Lub-de Hooge, PharmD, Department of Clinical Pharmacy and Pharmacology, University of Groningen, University Medical Center Groningen, P.O. Box 30001, 9700 RB Groningen, The Netherlands.
E-mail: m.n.de.hooge@umcg.nl
Published online Mar. 30, 2017.

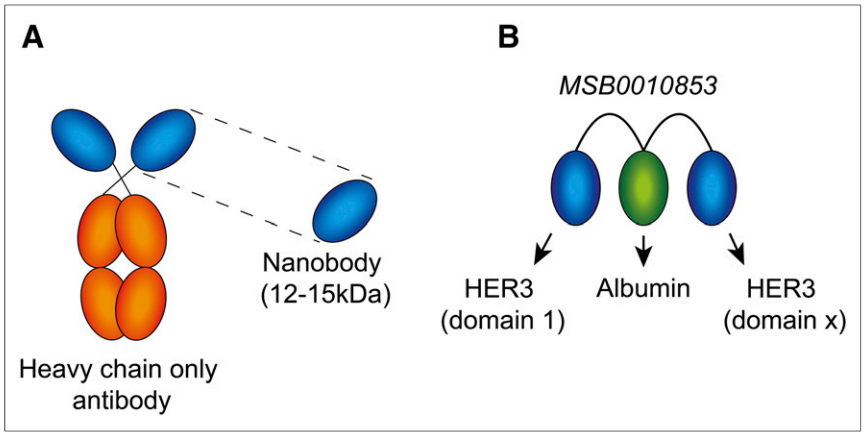

FIGURE 1. Composition of MSB0010853 (molecular weight, 39.5 kDa). (A) Nanobody is the variable domain of a heavy chain–only antibody. (B) MSB0010853 contains 3 Nanobodies that are linked together. The individual Nanobodies bind 2 different epitopes of HER3 and albumin. MSB0010853 binds HER3 at domain 1 and at a second unknown domain (defined as x).

imaging is currently used in drug development of monoclonal antibodies (*13*) and might facilitate decision making in future early clinical trials with MSB0010853. We radiolabeled MSB0010853 with ^{89}Zr, because the long half-life of ^{89}Zr (78.4 h) allows us to follow MSB0010853 in vivo and determine tumor uptake up to several days after injection.

The purpose of this study was to assess ^{89}Zr-MSB0010853 biodistribution and in vivo imaging in different HER3-expressing human tumor–bearing mouse models.

MATERIALS AND METHODS

Cell Lines

We used the non–small cell lung cancer cell line H441 (HER3-positive), head and neck squamous cell cancer cell line FaDu (HER3-positive), and non–small cell lung cancer cell line Calu-1 (HER3-negative), obtained from American Type Culture Collection (*14*). FaDu and H441 cells were cultured in Dulbecco modified Eagle medium (Invitrogen), supplemented with 10% fetal calf serum (Bodinco BV) and 2 mM L-glutamine (Invitrogen). Calu-1 was cultured in RPMI 1640 (Invitrogen) supplemented with 10% fetal calf serum and 2 mM L-glutamine. All cells were grown at 37°C in a fully humidified atmosphere containing 5% CO_2.

Synthesis and Quality Control of Conjugated and Radiolabeled ^{89}Zr-MSB0010853

MSB0010853 was formulated (10.24 mg/mL) in a buffer containing 20 nM L-histidine (Merck), 8% (w/v) sucrose (Calbiochem), and 0.01% (w/v) polysorbate 20 (Merck), pH 6.5. MSB0010853 was purified with water for injections (B. Braun), using a Vivaspin-2 10-kDa filter (GE Healthcare). MSB0010853 was reacted with a 4-fold molar excess of *N*-succinyldesferrioxamine-B-tetrafluorphenol-Fe (*N*-sucDf-TFP-Fe; ABX) as described previously (*15*). We used a different size-exclusion column (Superdex 75 10/300 GL column; GE Healthcare). Quality control was performed as described earlier (*16*). Because Fe^{3+} (in *N*-sucDf-TFP-Fe) absorbs light at 430 nm, we used size-exclusion high-performance liquid chromatography to determine the conjugation efficiency. Chelated MSB0010853 was stored in the original formulation buffer at −20°C and radiolabeled with ^{89}Zr (PerkinElmer) on the day of the experiments, as described previously (*15*). Radiochemical yields equaled the radiochemical purity after radiolabeling because purification was not necessary.

The binding of ^{89}Zr-MSB0010853 to human serum albumin (HSA [Sanquin]) was assessed in a competitive radioimmunoassay. Nunc-Immuno BreakApart enzyme-linked immunosorbent assay wells were incubated overnight at 4°C with 100 μL of HSA solution (30 μg/mL in bicarbonate buffer: 15 mM sodium carbonate [Merck], 35 mM sodium bicarbonate [Merck], pH 9.6), blocked with 1% skimmed milk powder (Fluka) in phosphate-buffered saline (PBS; 140 mmol/L NaCl, 9 mmol/L Na2HPO4, 1.3 mmol/L NaH2PO4; UMCG) at room temperature, and washed with 0.1% polysorbate 20 (Sigma-Aldrich) in PBS. ^{89}Zr-MSB0010853 (final concentration, 200 nM) was mixed with varying final concentrations of unlabeled MSB0010853 (2 nM to 2 μM). Dilution series were prepared using 1% skimmed milk powder and 0.1% polysorbate 20 in PBS. The wells were incubated with the solutions for 2 h. Hereafter, the wells were washed twice with 0.05% polysorbate 20 in PBS. Radioactivity was measured by a well-type LKB-1282-Compu-γ-system (LKB Wallac) and set to 100% for wells without nonlabeled MSB0010853. HSA affinity of ^{89}Zr-MSB0010853 was compared with unlabeled MSB0010853 by dividing the concentration of ^{89}Zr-MSB0010853 (200 nM) by the concentration of MSB0010853 needed to block 50% of ^{89}Zr-MSB0010853 binding to HSA.

Internalization experiments were started by harvesting 10^6 H441 cells with Accutase (Millipore) and suspending in 1% bovine serum albumin in PBS. Cells were incubated for 1 h on ice with 50 ng of ^{89}Zr-MSB0010853 with or without 4 μg of HSA. The excess of nonbound ^{89}Zr-MSB0010853 was removed and culture medium (4°C) added. Radioactivity was counted in a well-type γ-counter (LKB 1282 [CompuGamma]; membrane-bound activity at time zero [T0]). Hereafter, cells were incubated at 37°C or on ice for 1, 2, or 4 h, and medium was removed. Internalized (cell pellet) and membrane-bound ^{89}Zr-MSB0010853 (medium) were separated after 10-min incubation in 4 M urea buffer supplemented with 0.2 M glycine (pH 2). The internalized amount of radioactivity was calculated as a fraction of initial membrane-bound radioactivity at T0.

In Vitro HER3 Binding of ^{89}Zr-MSB0010853

The immunoreactivity of ^{89}Zr-MSB0010853 to HER3 was assessed with H441 cells in the cell-binding assay (*17*). Two series of H441 cell dilutions (50×10^6 cells/mL and 6.6×10^6 cells/mL) were incubated with ^{89}Zr-MSB0010853 (20 ng/mL) for 2 h at 4°C while being shaken. To 1 of the cell series, a more than 3,000-fold molar excess of MSB0010853 was added to correct for nonspecific binding. After 2 h of incubation, cells were washed twice with PBS containing 1% bovine serum albumin to reduce nonspecific tube binding. Cell-bound radioactivity was measured with a well-type γ-counter. Data obtained with 50×10^6 cells/mL ($n = 4$) were used to demonstrate that a more than 3,000-fold excess of nonlabeled MSB0010853 could block HER3 binding of ^{89}Zr-MSB0010853 (20 ng/mL).

Animal Studies

The institutional animal care and use committee of the University of Groningen approved all animal experiments. Animal studies were performed in male nude BALB/c mice (BALB/cOlaHsd-*Foxn1*^{nu} [Harlan]; 5–7 wk old at arrival). Animals were allowed to feed ad libitum, and experiments were performed under isoflurane inhalation anesthesia (induction, 5%; maintenance, 2%).

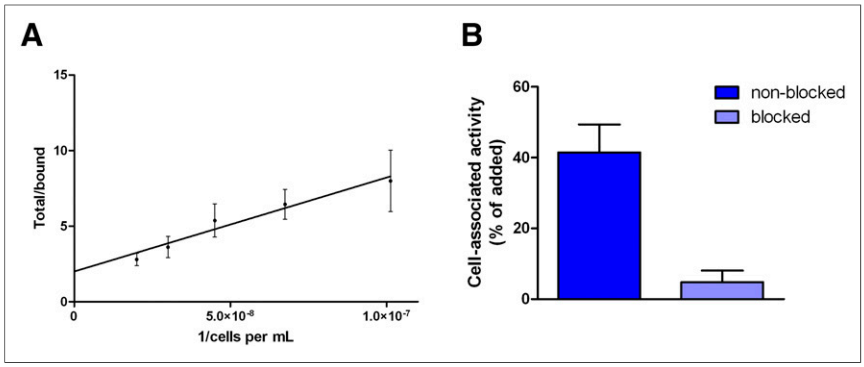

FIGURE 2. In vitro HER3 binding of ^{89}Zr-MSB0010853. (A) Reciprocal plot of ^{89}Zr-MSB0010853 binding to H441 cells to determine immunoreactivity. (B) In vitro blocking of ^{89}Zr-MSB0010853 HER3 binding on H441 tumor cells. Data are presented as mean ± SD (n = 4).

Tumor cells were harvested by trypsinization and diluted in PBS. Mice were injected subcutaneously in the flank with 4×10^6 H441, 5×10^6 FaDu, or 5×10^6 Calu-1 cells in 0.1 mL of PBS. Tumor growth was followed with caliper measurements. Tracer injection was performed 4–7 wk (H441), 3–5 wk (FaDu), or 19 wk (Calu-1) after tumor cell inoculation, when tumors were around 100–200 mm^3.

Protein Dose Escalation Biodistribution Study

Dose-dependent tumor uptake of ^{89}Zr-MSB0010853 was assessed in H441 tumor–bearing mice. Five dose groups of 5 μg (n = 5), 10 μg (n = 4), 25 μg (n = 5), 100 μg (n = 4), and 1,000 μg (n = 5) were included. ^{89}Zr-MSB0010853 was administered intravenously via penile injection, using a fixed volume of 150 μL. Four standards (5, 10, 15, and 20 μL) of the injected protein dose were stored to calculate the injected dose accurately. For the 5-, 10-, and 25-μg doses, no unlabeled MSB0010853 was mixed with ^{89}Zr-MSB0010853. For the 100-μg protein dose, 75 μg of unlabeled MSB0010853 were mixed with 25 μg of ^{89}Zr-MSB0010853. To reach 1,000 μg, 10 μg of ^{89}Zr-MSB0010853 were supplemented with 990 μg of unlabeled MSB0010853. One batch of N-sucDf-TFP–chelated MSB0010853 was used for radiolabeling. The specific activity of injected ^{89}Zr-MSB0010853 varied between 1 and 200 MBq/mg, as a fixed amount of radioactivity (1 MBq) was administered. For ex vivo biodistribution, animals were sacrificed 24 h after injection. Subsequently, organs and tissues were excised and weighed. Samples and standards were counted for radioactivity in a well-type γ-counter. Ex vivo tissue activity is expressed as percentage injected protein dose per gram of tissue (%ID/g).

PET Acquisition

Two mice were placed (one on top of the other) in a Focus 220 rodent scanner (CTI Siemens), with the tumor in the field of view. Mice were kept warm on heating mats. Acquisition times differed between 10 min (24-h time point) and 75 min (96-h time point). A transmission scan of 515 s was obtained using a ^{57}Co point source to correct for tissue attenuation.

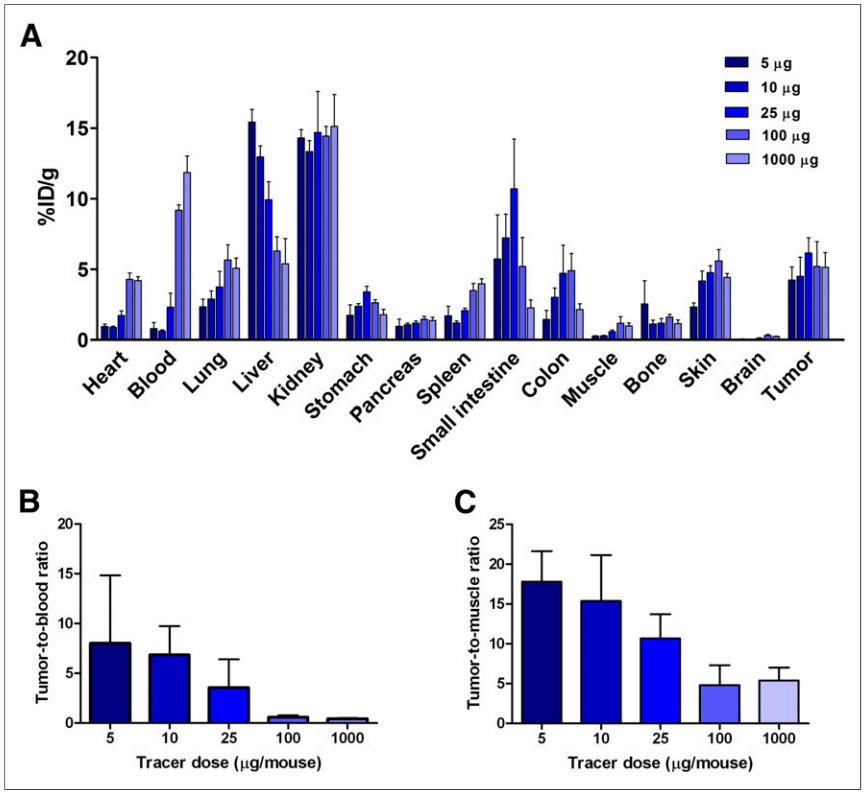

FIGURE 3. Protein dose–dependent ex vivo biodistribution of ^{89}Zr-MSB0010853 in mice bearing H441 tumors injected with 5, 10, 25, 100, or 1,000 μg at 24 h after tracer injection, expressed as %ID/g (A), tumor-to-blood ratios (B), and tumor-to-muscle ratios (C). Data are presented as mean ± SD (n = 4–5).

Time-Dependent Biodistribution and Small-Animal Imaging of ^{89}Zr-MSB0010853

Time-dependent biodistribution of ^{89}Zr-MSB0010853 (25 μg, 1–5 MBq = 40–200 MBq/mg) was evaluated in H441 tumor–bearing mice at 3, 6, 24, or 96 h after injection (n = 4–6). One batch of N-sucDf-TFP–chelated MSB0010853 was radiolabeled with ^{89}Zr for each time point separately. Small-animal PET images were obtained 24, 48, 72, and 96 h after injection of 25 μg of ^{89}Zr-MSB0010853 (5 MBq = 200 MBq/mg, n = 5). PET data were reconstructed using a 2-dimensional ordered-subset expectation maximization reconstruction algorithm with Fourier rebinning, 4 iterations and 16 subsets. Images were quantified using Amide's medical image data examiner software (version 1.0.4; Stanford University). Regions of interest were drawn for tumors at 50% of maximum intensity, and images were quantified using Amide's medical image data examiner software. The data are presented as the SUV_{mean} or SUV_{max}.

Small-Animal PET Imaging and Biodistribution in Different Tumor Models

Mice bearing FaDu, H441, or Calu-1 tumors were scanned 24 h after injection of 25 μg of ^{89}Zr-MSB0010853 (1 MBq = 40 MBq/mg;

n = 3–5/group). After scanning, mice were sacrificed for ex vivo biodistribution analysis.

Statistical Analysis

Data are presented as mean ± SD. Statistical analysis between 2 nonparametric groups was performed using the Mann–Whitney U test (Prism 5; GraphPad). P values of 0.05 or less were considered significant.

RESULTS

^{89}Zr-MSB0010853 Production and Quality Control

On average, 1 mol of *N*-sucDf-TFP-Fe was conjugated to 1 mol of MSB0010853. After MSB0010853 was labeled with ^{89}Zr, the radiochemical purity and radiochemical yields were greater than 95%. Size-exclusion high-performance liquid chromatography analyses did not show any fragmentation or aggregation of the ^{89}Zr labeled MSB0010853 (Supplemental Fig. 1; supplemental materials are available at http://jnm.snmjournals.org). The relative affinity to HSA of ^{89}Zr-MSB0010853 compared with unlabeled MSB0010853 was 67% ± 9%. A small amount of ^{89}Zr-MSB0010853 was internalized within 4 h of incubation, 5.5% ± 11.3% in the absence of HSA and 12.2% ± 9.6% in the presence of HSA (Supplemental Fig. 2).

In Vitro HER3 Binding of ^{89}Zr-MSB0010853

The immunoreactive fraction of ^{89}Zr-MSB0010853 against HER3 on H441 cells was 0.68 ± 0.11 (Fig. 2A). HER3-specific binding of ^{89}Zr-MSB0010853 could be blocked with an excess of unlabeled MSB0010853 (Fig. 2B).

Protein Dose Escalation Biodistribution Study

Protein dose escalation biodistribution studies in H441-xenografted mice showed comparable tumor uptake of ^{89}Zr-MSB0010853 in all tested dose groups, ranging between 4.3 and 5.7 %ID/g (Fig. 3A). Tumor-to-blood and tumor-to-muscle ratios, however, decreased from, respectively, 8.0 ± 6.8 to 0.6 ± 0.2 and 17.8 ± 3.9 to 4.8 ± 2.5, when the protein dose was increased from 5 to 100 μg (Figs. 3B and 3C). Both tumor-to-blood and tumor-to-muscle ratios did not further decrease by increasing the protein dose to 1,000 μg. Renal uptake was protein dose–independent, ranging between 14.3 and 15.4 %ID/g. Blood levels of ^{89}Zr-MSB0010853 correlated with the administered dose, which was lowest in the 5-μg dose group (0.8 ± 0.4 %ID/g) and 15-fold higher in the 1,000-μg protein dose group (12.1 ± 1.1 %ID/g). In most organs, uptake increased with increasing protein doses (up to 25–100 μg). Liver uptake negatively correlated with the administered dose, which was highest in the 5-μg protein dose group (15.4 ± 0.9 %ID/g) and 2.8-fold lower in the 1,000-μg protein dose group (5.5 ± 1.8 %ID/g). Because 25 μg of ^{89}Zr-MSB0010853 resulted in relatively high tumor uptake and low blood levels, further animal studies were performed using this protein dose.

Time-Dependent Biodistribution and Small-Animal PET Imaging of ^{89}Zr-MSB0010853

Up to 24 h after injection, tumor uptake of ^{89}Zr-MSB0010853 increased in time (to 6.2 ± 1.1 %ID/g), which decreased subsequently (Fig. 4A). ^{89}Zr-MSB0010853 rapidly cleared from the bloodstream, resulting in tumor-to-blood ratios increasing in time up to 33.1 ± 7.9 at 96 h after tracer injection (Fig. 4B). In addition, tumor-to-muscle ratios increased up to 96 h after injection to 13.4 ± 5.3 (Fig. 4C).

Although ^{89}Zr-MSB0010853 showed minimal internalization in H441 cells in vitro (Supplemental Fig. 2), H441 tumors were still clearly visible up to 96 h after injection (Fig. 5). The highest SUV_{mean} (0.6 ± 0.2) was observed 24 h after injection, decreasing subsequently (Fig. 5B).

Small-Animal PET Imaging and Biodistribution in Different Tumor Models

Tumor uptake of ^{89}Zr-MSB0010853 could be visualized 24 h after injection in HER3-expressing H441 and FaDu xenografts. Less tumor uptake was observed in HER3-negative Calu-1 xenografts (Fig. 6A). Because Calu-1 cells do not express HER3, tumor uptake of ^{89}Zr-MSB0010853 in Calu-1 tumors is nonspecific. Ex vivo biodistribution data confirmed this observation. Tumor uptake in the HER3-negative Calu-1 model was 2.3 ± 0.3 %ID/g, which was 2.4-fold lower than in HER3-positive H441 (6.2 ± 1.1 %ID/g; P = 0.04) and 2.2-fold lower than in FaDu (5.1 ± 0.4 %ID/g; P = 0.04) xenografts (Fig. 6B).

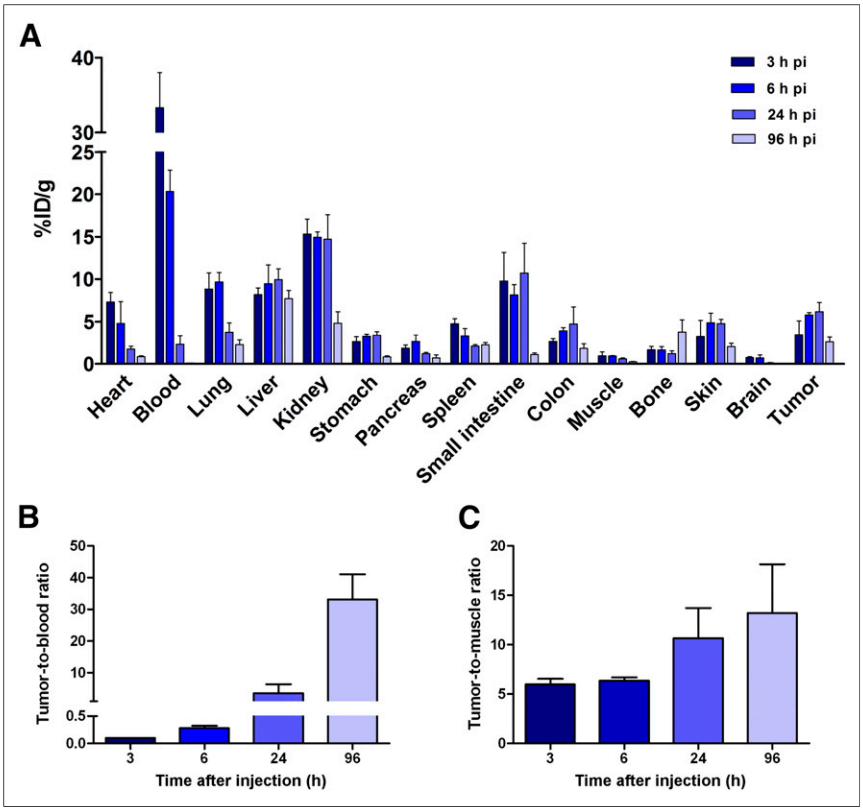

FIGURE 4. Time-dependent ex vivo biodistribution of ^{89}Zr-MSB0010853 in mice bearing H441 xenografts injected with 25 μg of ^{89}Zr-MSB0010853 at 3, 6, 24, and 96 h after tracer injection, expressed as %ID/g (A), tumor-to-blood ratios (B), and tumor-to-muscle ratios (C). Data are presented as mean ± SD (n = 4–6). pi = after injection.

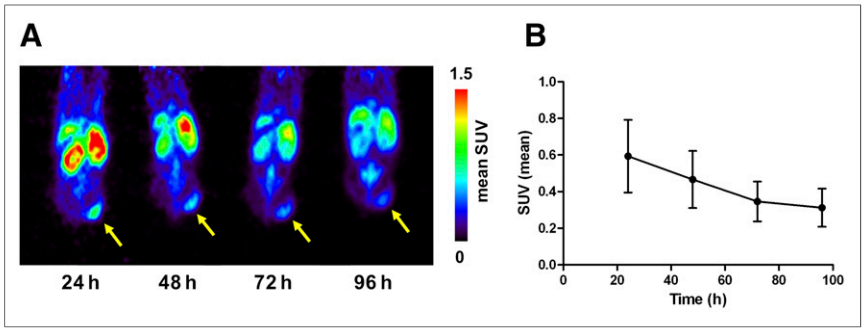

FIGURE 5. (A) Representative coronal PET images of mice bearing H441 xenografts injected with 25 μg of ^{89}Zr-MSB0010853 obtained at 24, 48, 72, and 96 h after tracer injection. (B) Small-animal PET data quantification was performed for tumor uptake at 24, 48, 72, and 96 h after tracer injection in all mice. Data are presented as mean ± SD (n = 5).

DISCUSSION

To our knowledge, this is the first report describing dose- and time-dependent biodistribution of a biparatopic anti-HER3 Nanobody construct in mice. With small-animal PET imaging, biodistribution and tumor uptake of ^{89}Zr-MSB0010853 were visualized up to at least 96 h after injection. This study illustrated that PET imaging with ^{89}Zr-MSB0010853 provides noninvasive information on MSB0010853 biodistribution and tumor uptake.

We demonstrated that tissue distribution of ^{89}Zr-MSB0010853 in mice is dose-dependent. At 24 h after injection, ^{89}Zr-MSB0010853 blood levels in the 1,000-μg dose group were 15-fold higher than in the 5-μg dose group. This increase might be due to saturation of hepatic uptake of ^{89}Zr-MSB0010853, because hepatic uptake inversely correlated with blood levels. Increasing the protein dose of an albumin-binding antihepatocyte growth factor Nanobody construct (*18*) and an albumin-binding anti-HER2 Affibody construct (*19*) did not affect liver uptake. Therefore, saturation of ^{89}Zr-MSB0010853 liver uptake was not due to in vivo albumin binding. Because MSB0010853 is cross-reactive with mouse HER3 and HER3 is expressed on hepatocytes and bile duct cells in the liver, saturation is more likely due to intrahepatic HER3 binding (*20*). In line with our results, saturation of HER3-dependent liver uptake was also observed in mice injected with ^{99m}Tc-labeled anti-HER3 Affibody molecules, cross-reactive for mouse HER3 (^{99m}Tc(CO)3-Z08699-H6 and ^{99m}Tc(CO)3-HEHEHE-ZHER3:08699) (*21,22*). However, saturation of the liver did not increase blood levels of ^{99m}Tc(CO)3-Z08699-H6 and ^{99m}Tc(CO)3-HEHEHE-ZHER3:08699, 4–6 h after injection. This was likely due to the fast clearance of these small anti-HER3 Affibody molecules, without albumin-binding capacity that extends half-life.

Apart from the liver, saturation of ^{89}Zr-MSB0010853 was also observed in other organs that express HER3, such as the lung, stomach, small intestines, colon, and skin (*18*). Uptake of ^{89}Zr-MSB0010853 in these organs increased with increasing protein doses up to 25–100 μg. This might well be due to increased delivery of the tracer to these tissues, given the increased tracer blood levels. At higher protein doses, blood levels continued to increase whereas uptake in these HER3-expressing organs did not, indicating saturation of HER3-dependent organ uptake. We additionally observed saturation of HER3-specific tumor uptake. This can best be perceived from Figures 3B and 3C. Increasing the protein dose resulted in a decreased tumor-to-blood and tumor-to-muscle ratio. If tumor uptake of ^{89}Zr-MSB0010853 was solely due to nonspecific uptake, the drastic 15-fold increase in blood levels would promote tumor uptake.

Renal uptake of ^{89}Zr-MSB0010853 is relatively low (<15 %ID/g) as compared with HER3-targeting ^{99m}Tc(CO)3-Z08699-H6 and ^{99m}Tc(CO)3-HEHEHE-ZHER3:08699 (>70 %ID/g) (*21,22*). However, it is comparable with the renal uptake of ^{177}Lu-aEGFR-aEGFR-aAlb, a similar-sized EGFR binding Nanobody construct with albumin-binding capacity (*23*). Additionally, blood radioactivity levels of ^{177}Lu-aEGFR-aEGFR-aAlb and ^{89}Zr-MSB0010853 were also comparable (~10 %ID/g) at 24 h after injection in mice. Injected protein doses were similar for both tracers (100 μg), demonstrating a similar effect of albumin binding on half-life extension of both Nanobody constructs. The half-life of murine serum albumin in mice is 1.1–1.6 d, much shorter than the half-life of 15–19 d for HSA in humans (*24–27*). Therefore, we expect a slower clearance of ^{89}Zr-MSB0010853 in humans than in mice, allowing a longer ^{89}Zr-MSB0010853 accumulation time in tumors of patients, likely resulting in higher tumor accumulation in patients than in mice.

PET imaging is increasingly used in the development of targeting agents (*13*). It could provide useful information about the pharmacologic behavior and tumor-targeting properties of these agents, facilitating patient selection and the management of clinical dose-finding studies (*13,28*). PET imaging in patients will likely give us additional information on MSB0010853 in vivo behavior and tumor targeting. The presence of target does not mean that targeted drugs are able to accumulate in target-positive tumors (*29*). This may be due to many factors such as tumor perfusion, presence of stroma, tumor interstitial fluid pressure, and anatomic location of the tumor (*29*). Although the level of tumor accumulation is currently missing in many early-phase clinical trials, it is obtainable by including PET imaging in these studies.

Preclinical and clinical PET imaging has also been used in the development of

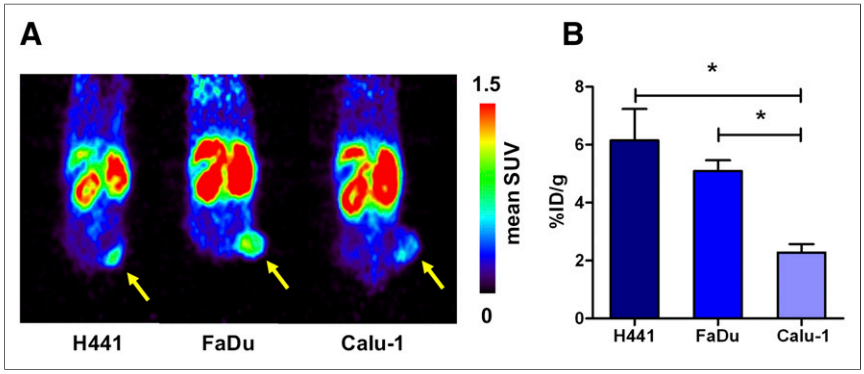

FIGURE 6. Representative coronal PET images of mice bearing H441, FaDu, or Calu-1 xenografts 24 h after injection of 25 μg of ^{89}Zr-MSB0010853 (A), with corresponding tumor uptake (B). Data are presented as mean ± SD (n = 3–5). *$P \leq 0.05$, Mann–Whitney.

RG7116 and patritumab, 2 intact anti-HER3 antibodies. Preclinical biodistribution studies in mice showed HER3-specific tumor uptake of both radiolabeled antibodies (*14,30*). Compared with ^{89}Zr-MSB0010853, maximum ^{89}Zr-RG7116 tumor uptake at 6 d after injection was higher, with 19.0, 13.9, and 7.6 %ID/g in H441, FaDu, and Calu-1 xenografts. This could be due to a high amount of nonspecific ^{89}Zr-RG7116 tumor uptake, because uptake of control ^{111}In-IgG in these tumors was, respectively, 16.5, 9.1 and 8.3 %ID/g (*14*). Because ^{89}Zr-RG7116 is not cross-reactive for mouse HER3, it lacks specific organ binding. Therefore, tumor-to-organ ratios were higher than observed with ^{89}Zr-MSB0010853. However, tumor-to-blood ratios were comparable. Preliminary results with ^{64}Cu-labeled patritumab and ^{89}Zr-RG7116 in patients show that biodistribution and tumor uptake of HER3-targeting agents can noninvasively be visualized with whole-body PET imaging (*31,32*). Differences in species (humans vs. mice) and the expected longer circulation time of ^{89}Zr-MSB0010853 in humans preclude quantitative comparison with our preclinical ^{89}Zr-MSB0010853 findings.

CONCLUSION

Biodistribution of ^{89}Zr-MSB0010853 is protein dose– and time-dependent and can be studied noninvasively using PET imaging. In addition, tumor uptake of ^{89}Zr-MSB0010853 correlated with HER3 expression. As demonstrated in our study, PET imaging gives noninvasive insight into the in vivo behavior of MSB0010853. In early-phase clinical trials, ^{89}Zr-MSB0010853 can potentially be used to study biodistribution and tumor uptake of MSB0010853 in cancer patients to facilitate clinical development.

DISCLOSURE

This work was supported by Merck Biopharma. Christine Knuehl is employed by Merck Biopharma and Maarten van Roy is employed by Ablynx N.V. No other potential conflicts of interest were disclosed by the other authors.

REFERENCES

1. Citri A, Yarden Y. EGF-ERBB signalling: towards the systems level. *Nat Rev Mol Cell Biol.* 2006;7:505–516.
2. Lipton A, Goodman L, Leitzel K, et al. HER3, p95HER2, and HER2 protein expression levels define multiple subtypes of HER2-positive metastatic breast cancer. *Breast Cancer Res Treat.* 2013;141:43–53.
3. Huang S, Li C, Armstrong EA, et al. Dual targeting of EGFR and HER3 with MEHD7945A overcomes acquired resistance to EGFR inhibitors and radiation. *Cancer Res.* 2013;73:824–833.
4. Jiang N, Wang D, Hu Z, et al. Combination of anti-HER3 antibody MM-121/SAR256212 and cetuximab inhibits tumor growth in preclinical models of head and neck squamous cell carcinoma. *Mol Cancer Ther.* 2014;13:1826–1836.
5. Iida M, Brand TM, Starr MM, et al. Overcoming acquired resistance to cetuximab by dual targeting HER family receptors with antibody-based therapy. *Mol Cancer.* 2014;13:242.
6. Mirschberger C, Schiller CB, Schraml M, et al. RG7116, a therapeutic antibody that binds the inactive HER3 receptor and is optimized for immune effector activation. *Cancer Res.* 2013;73:5183–5194.
7. Huang J, Wang S, Lyu H, et al. The anti-erbB3 antibody MM-121/SAR256212 in combination with trastuzumab exerts potent antitumor activity against trastuzumab-resistant breast cancer cells. *Mol Cancer.* 2013;12:134.
8. Garrett JT, Sutton CR, Kuba MG, Cook RS, Arteaga CL. Dual blockade of HER2 in HER2-overexpressing tumor cells does not completely eliminate HER3 function. *Clin Cancer Res.* 2013;19:610–619.
9. Kol A, Terwisscha van Scheltinga AG, Timmer-Bosscha H, et al. HER3, serious partner in crime: therapeutic approaches and potential biomarkers for effect of HER3-targeting. *Pharmacol Ther.* 2014;143:1–11.
10. D'Souza JW, Reddy S, Goldsmith LE, et al. Combining anti-ERBB3 antibodies specific for domain I and domain III enhances the anti-tumor activity over the individual monoclonal antibodies. *PLoS One.* 2014;9:e112376.
11. Oliveira S, Heukers R, Sornkom J, Kok RJ. van Bergen en Henegouwen PM. Targeting tumors with nanobodies for cancer imaging and therapy. *J Control Release.* 2013;172:607–617.
12. Chakravarty R, Goel S, Cai W. Nanobody: the "magic bullet" for molecular imaging? *Theranostics.* 2014;4:386–398.
13. Lamberts LE, Williams SP, Terwisscha van Scheltinga AG, et al. Antibody positron emission tomography imaging in anticancer drug development. *J Clin Oncol.* 2015;33:1491–1504.
14. Terwisscha van Scheltinga AG, Lub-de Hooge MN, Abiraj K, et al. ImmunoPET and biodistribution with human epidermal growth factor receptor 3 targeting antibody ^{89}Zr-RG7116. *MAbs.* 2014;6:1051–1058.
15. Verel I, Visser GW, Boellaard R, Stigter-van Walsum M, Snow GB, van Dongen GA. ^{89}Zr immuno-PET: comprehensive procedures for the production of ^{89}Zr-labeled monoclonal antibodies. *J Nucl Med.* 2003;44:1271–1281.
16. Nagengast WB, de Vries EG, Hospers GA, et al. In vivo VEGF imaging with radiolabeled bevacizumab in a human ovarian tumor xenograft. *J Nucl Med.* 2007;48:1313–1319.
17. Lindmo T, Boven E, Cuttitta F, Fedorko J, Bunn PA. Determination of the immunoreactive fraction of radiolabeled monoclonal antibodies by linear extrapolation to binding at infinite antigen excess. *J Immunol Methods.* 1984;72:77–89.
18. Vosjan MJ, Vercammen J, Kolkman JA, Stigter-van Walsum M, Revets H, van Dongen GA. Nanobodies targeting the hepatocyte growth factor: potential new drugs for molecular cancer therapy. *Mol Cancer Ther.* 2012;11:1017–1025.
19. Orlova A, Jonsson A, Rosik D, et al. Site-specific radiometal labeling and improved biodistribution using ABY-027, a novel HER2-targeting affibody molecule-albumin-binding domain fusion protein. *J Nucl Med.* 2013;54:961–968.
20. ERBB3 tissue atlas. The human protein atlas website. http://www.proteinatlas.org/ENSG00000065361-ERBB3/tissue. Accessed April 10, 2017.
21. Malm M, Kronqvist N, Lindberg H, et al. Inhibiting HER3-mediated tumor cell growth with affibody molecules engineered to low picomolar affinity by position-directed error-prone PCR-like diversification. *PLoS One.* 2013;8:e62791.
22. Orlova A, Malm M, Rosestedt M, et al. Imaging of HER3-expressing xenografts in mice using a ^{99m}Tc(CO)$_3$-HEHEHE-$Z_{HER3:08699}$ affibody molecule. *Eur J Nucl Med Mol Imaging.* 2014;41:1450–1459.
23. Tijink BM, Laeremans T, Budde M, et al. Improved tumor targeting of anti-epidermal growth factor receptor nanobodies through albumin binding: taking advantage of modular nanobody technology. *Mol Cancer Ther.* 2008;7:2288–2297.
24. Dixon FJ, Maurer PH, Deichmiller MP. Half-lives of homologous serum albumins in several species. *Proc Soc Exp Biol Med.* 1953;83:287–288.
25. Chaudhury C, Mehnaz S, Robinson JM, et al. The major histocompatibility complex-related fc receptor for IgG (FcRn) binds albumin and prolongs its lifespan. *J Exp Med.* 2003;197:315–322.
26. Andersen JT, Pehrson R, Tolmachev V, Daba MB, Abrahmsen L, Ekblad C. Extending half-life by indirect targeting of the neonatal fc receptor (FcRn) using a minimal albumin binding domain. *J Biol Chem.* 2011;286:5234–5241.
27. Peters T. Metabolism: albumin in the body. In: *All About Albumin: Biochemistry, Genetics and Medical Applications.* San Diego, CA: Academic Press; 1995:188–250.
28. Ciprotti M, Tebbutt NC, Lee FT, et al. Phase I imaging and pharmacodynamic trial of CS-1008 in patients with metastatic colorectal cancer. *J Clin Oncol.* 2015;33:2609–2616.
29. de Vries EG, de Jong S, Gietema JA. Molecular imaging as a tool for drug development and trial design. *J Clin Oncol.* 2015;33:2585–2587.
30. Sharp TL, Glaus C, Fettig N, et al. Pharmacological evaluation of ^{64}Cu-DOTA-AMG888 (U3-1287) in control and tumor bearing mice using biodistribution and microPET imaging. Abstract presented at: The 2011 World Molecular Imaging Congress; September 7–11, 2011; San Diego, CA.
31. Bensch F, Lamberts LE, Lub-de Hooge MN, et al. Phase I imaging study of the HER3 antibody RG7116 using 89Zr-RG7116-PET in patients with metastatic or locally advanced HER3-positive solid tumors [abstract]. *J Clin Oncol.* 2014;32 (suppl):11095.
32. Lockhart IC, Liu Y, Dehdashti F, et al. A phase 1 evaluation of ^{64}Cu-DOTA-patritumab to assess dosimetry, receptor occupancy, and safety in advanced solid tumors [abstract]. *Cancer Res.* 2014;74(19, Suppl)5443.